Article
Vol. 23, No. 1, p. 59–68, February 2019
https://doi.org/10.1007/s12303-018-0010-7
pISSN 1226-4806 eISSN 1598-7477
Geosciences Journal GJ

Cosmogenic nuclides (^{10}Be and ^{26}Al) erosion rate constraints in the Badain Jaran Desert, northwest China: implications for surface erosion mechanisms and landform evolution

Tong Zhao[1,2,3], Wenjing Liu[1,2,3,4]*, Zhifang Xu[1,2,3], Taoze Liu[5], Sheng Xu[6], Lifeng Cui[5], and Chao Shi[3]

[1]Key Laboratory of Cenozoic Geology and Environment, Institute of Geology and Geophysics, Chinese Academy of Sciences, Beijing 100029, China
[2]CAS Center for Excellence in Life and Paleoenvironment, Beijing 100044, China
[3]University of Chinese Academy of Sciences, Beijing 100049, China
[4]Earth and Environmental Systems Institute and Department of Geosciences, Pennsylvania State University, University Park, PA 16802, USA
[5]State Key Laboratory of Environmental Geochemistry, Institute of Geochemistry, Chinese Academy of Sciences, Guiyang, Guizhou 550002, China
[6]Scottish Universities Environmental Research Center, East Kilbride, G75 0QF, UK

ABSTRACT: Both tectonics and climate affect surface erosion and change the landform. Long-term surface erosion rates determined by in situ produced cosmogenic nuclides are useful quantitative constraints for landform evolution in geological time scale. Measurements of cosmogenic ^{10}Be and ^{26}Al in the granitic rocks exposed in the Badain Jaran Desert, give a mean erosion rate of 7.3 ± 2.6 m/Ma, which is an order of magnitude higher than those reported in other extremely arid regions. Tectonic activity is supposed to be the first order control on regional erosion rate by comparing the ^{10}Be erosion rates of arid regions with different precipitation ranges and tectonic activities worldwide. However the higher erosion rates in the Badain Jaran Desert compared with other arid regions within the stable tectonic background were attributed to the wind erosion and periodically warmer and wetter climate since late Pleistocene. Besides, the estimated eroded mass flux of 7.8×10^4 t/y suggests that erosion products of bedrocks in the Badian Jaran Desert only contribute minor desert deposits, which indicates massive exogenous materials input to the desert.

Key words: cosmogenic nuclides, Badain Jaran Desert, erosion rate, erosion mechanisms, landform evolution

Manuscript received May 9, 2017; Manuscript accepted January 23, 2018

1. INTRODUCTION

The understanding of landscape evolution has been limited by the lack of data on surface erosion rates over appropriate geologic time scales (Lal, 1991; Small et al., 1997; Cockburn et al., 1999; Wateren and Dunai, 2001; Bierman and Caffee, 2002). The thermochronologic methods derived from the application of mineral cooling ages or fission-track data, could obtain exhumation rates which result from exhumation and exposure of rocks from deeper levels, on millions of years. However, the exhumation rate data is strongly sensitive to the assumed geothermal gradient (Lal et al., 2004), and these methods rarely evaluate landform evolution in terrains where landscapes change very slowly and/or at time scales of 10^4–10^6 y. Cosmogenic nuclides methods, which could measure exposure ages up to millions of years and long-term erosion rates as low as a decimeter per million years, could supply an age estimation at the time gap of 10^4–10^6 y, embracing the duration of Quaternary (Fujioka and Chappell, 2011), and have been widely used in recent researches of desert landscapes and late Cenozoic climate changes (Small et al., 1997; Cockburn et al., 1999; Bierman and Caffee, 2002; Kong et al., 2007; Placzek et al., 2010).

Long-term erosion rates and exposure ages across various temporal and spatial scales provided by cosmogenic nuclides methods are quantitative constraints for continental landscape evolution and surface process research. Cockburn et al. (1999) used in situ cosmogenic ^{10}Be and ^{26}Al to examine denudation

*Corresponding author:
Wenjing Liu
Key Laboratory of Cenozoic Geology and Environment, Institute of Geology and Geophysics, Chinese Academy of Sciences, No. 19, Beitucheng Western Road, Chaoyang District, Beijing 100029, China
Tel: +86-10-82998289, E-mail: wul26@psu.edu

rates on inselberg summit in central Namib Desert, their results indicate that regional denudation has amounted to more than 50 m over the past 10 Ma. Fujioka et al. (2005) measured ^{10}Be and ^{21}Ne exposure ages of silcrete clasts in central Australia, proposed that soils were tripped and silcrete was exhumed with the onset of aridity, and concluded that stony deserts in the central Australia began to form at ~4 Ma, the transition coincide with the onset of the Quaternary ice ages and global cooling. In addition, cosmogenic erosion rates in different geomorphic settings could contribute to a better understanding to distinguish the response of landform erosion to tectonic and climatic forcing. A compilation of world-wide erosion rates in non-glaciated areas from von Blanckenburg (2005) implied an explicit correlation with tectonic activities (such as faulting, escarpment formation and retreat, rifting, surface uplift), on the contrary, no obvious relationship exists between erosion rates and climate parameters such as precipitation and temperature. The arid northern Flinders Ranges, humid Northern Territory of northern Australia and semi-arid Davenport Range, in which neotectonic activities are from active to sparse, the ^{10}Be concentrations in granites or quartzite bedrock surfaces indicate erosion rates of ~14 m/Ma, 2–4 m/Ma and 0.3 m/Ma, respectively (Quigley et al., 2007; Bierman and Caffee, 2002; Belton et al., 2004). Tectonic activity was demonstrated to play a more important role in controlling surface erosion in arid regions in many studies (Cockburn et al., 2000; Kong et al., 2007; Quigley et al., 2007). However, the temporal and spatial variation of climatic conditions dominate surface erosion rate in stable areas where tectonic forcing is negligible. Placzek et al. (2010) measured cosmogenic ^{10}Be, ^{26}Al and ^{21}Ne of the boulder fields, the most stable landscape elements in the Central Atacama, the exposure ages of the boulders indicate that the Central Atacama surface erosion closely dependent on episodic Pliocene and Pleistocene rainfall. Granite bedrock ^{10}Be erosion rates in stable Australia terrain, on the order of 1–3 m/Ma, show positive correlation with mean annual precipitations (MAP) (Bierman and Caffee, 2002). Wateren and Dunai (2001) also found that accelerated erosion rates in Namib Desert were strongly related to early Pleistocene climatic change.

In this paper, long-term erosion rates from in situ produced cosmogenic ^{10}Be and ^{26}Al concentrations in the Badain Jaran Desert were estimated for the first time. Influenced by the fluctuation of East Asia monsoon, winter monsoon and westerlies, the Badain Jaran Desert went through the alternation of wet warm and dry cold climate since late Pleistocene (Yang et al., 2004; An et al., 2006; Gao et al., 2006; Yang et al., 2010; Ma et al., 2012). The peneplain landscape in the interior desert indicates a stable tectonic background here (Gao et al., 2013). Therefore the tectonically stable settings with shifting climate history provide good background for exploring climate impact to surface erosion. Quantifying the surface erosion rates in the Badain Jaran Desert may provide constraints for landform evolution and interpretations of tectonic and climatic control on erosion rate on this vast arid land.

2. STUDY AREA

The Badain Jaran Desert which situated at the northeast Tibetan Plateau, bounded by Baida Mountains and Yabulai Mountains to the south and east and by lowlands and lake basins to the west and north, covers an area of 49200 km^2 (Fig. 1). The Badain Jaran Desert is characterized by an extremely arid climate, with cold winters and moderately warm summers. The prevailing wind is westerly wind, and the annual mean wind velocity ranges from 2.8 to 4.6 m/s (Zhang et al., 2015). Regional precipitation and temperature present the regularity of spatial and temporal distribution because of Asian summer monsoon. The average annual precipitation and temperature range from 118 mm and 7.7 °C in the southeast to 37 mm and 8.2 °C in the northwest. More than half of the precipitation happens in June to August (Yang et al., 2010). The vegetation is not well developed due to low precipitation. The altitude of the desert varies between 1600 m in the southeast and 900 m in the northwest. 70–80% of this area is covered by active dunes (Dong et al., 2016), the tallest mega-dunes in the world are distributed densely in the southeast, and most of these dunes are higher than 100 m (Liu et al., 2015). Numerous permanent lakes with no surface runoff occur between the large dunes, the dunes decrease in size and lakes gradually disappear towards the northwest desert.

The extension of northeast Tibetan plateau produced an elongated mountains and basins and induced E–NE striking fault zone in the south and east edges of the desert, such as Yabulai Mountain fault, which runs for 120 km along the Yabulai Mountains. Investigations of the fault indicate that fault activities since Pleistocene have been demonstrated (Darby et al., 2005; Chen and Xu, 2006; Yu et al., 2013), Quaternary to recent fault vertical slip rate is ~110 m/Ma, and the latest recorded seismic event occurred in 1.5 ka BP (Yu et al., 2013). The vast interior desert with few seismic activity records, characterized by peneplain landscape and low residual hills, is tectonically stable (Gao et al., 2013). The outcrop samples, collected on two large granite intrusive bodies in Yabulai-Shan and Zongnai-Shan regions (Fig. 1) are predominantly Indosinian biotite granite and monzonitic granite.

3. METHODS

3.1. Sampling

Sampling strategy is crucial for cosmogenic methods, sampling

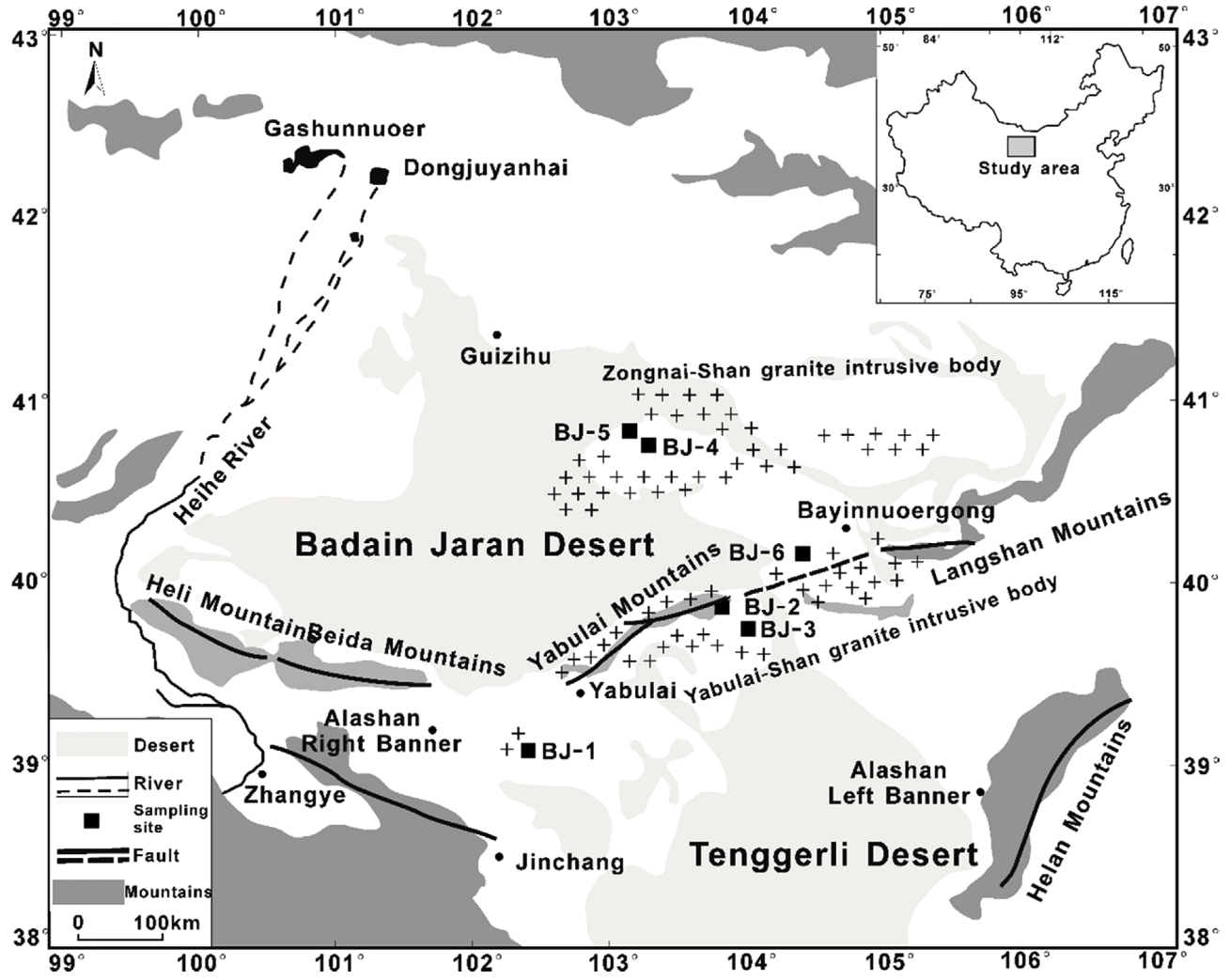

Fig. 1. Sketch of the Badain Jaran Desert and sampling locations (modified from Yang et al., 2010).

in one region but various rock types and landforms may cause different results. For example, the ^{10}Be erosion rates of granite inselbergs (5 m/Ma, Cockburn et al., 1999) and exposed quartz veins (~1 m/Ma, Wateren and Dunai, 2001) in Namib Desert are significantly different. The landscape of the Badain Jaran Desert mainly consists of active dune field, surrounded by desert plain with pediments on the margin (Yang et al., 2000). Six granitic rocks were collected on flat bedrock surface for measurement of in situ produced cosmogenic nuclides. Five rocks (Fig. 2) were at the desert plain, and one at the Yabulai Mountain front (BJ-2). The many granite outcrops at the desert plain display different weathering forms, such as Tafoni (Fig. 2c). At least three rocks from each site were collected as one sample to reduce the deviation of rates by episodic erosion.

3.2. Cosmogenic Nuclide Theory

The terrestrial cosmogenic nuclides, which are produced when high-energy particles interact with Earth's soil and rocks including ^{10}Be, ^{26}Al, ^{21}Ne, ^{36}Cl, ^{14}C, ^{53}Mn, used to determine exposure ages and erosion rates in geomorphological studies. Among these, two nuclides (^{10}Be and ^{26}Al) with contrasting decay rates and half-lives (1.387 Ma for ^{10}Be and 0.705 Ma for ^{26}Al respectively, Norris et al., 1983; Chmeleff et al., 2010; Korschinek et al., 2010) have been widely used to determine the exposure history of rocks. The concentrations of the cosmogenic nuclides are defined by two free parameters, erosion rate (ε) and exposure time (T) (Lal, 1991), as follow:

$$N = \frac{P}{\lambda + \varepsilon\rho/\Lambda}\left(1 - e^{-(\lambda + \varepsilon\rho/\Lambda)t}\right), \quad (1)$$

where ρ is the rock density (g/cm^3) and Λ is the attenuation length (g/cm^2); λ is the decay constant of the nuclide; P is the production rate (atoms/g/a), and N is the measured concentration (atoms/g). The erosion rate can be calculated in this equation when surface was continually exposed and steadily eroded for

https://doi.org/10.1007/s12303-018-0010-7

Fig. 2. Sampling site photos. Landscape of the edge (a and f) and the interior (d and e) of the desert plain. Many granite outcrops display different weathering forms, such as Tafoni (c, near the BJ-3) and hemispherical granite (f).

sufficient time $T >> 1/(\lambda + \rho\varepsilon/\Lambda)$ and nuclide concentrations have reached steady state.

3.3. Sample Preparation

Samples were first crushed and sieved to 0.25–0.425 mm size, and 20–30 g pure quartz was extracted by magnetic separation and repeated chemical dissolution with a mixed solution of dilute HF and HNO_3 (Kohl and Nishiizumi, 1992). Pure quartz were completely dissolved in hydrofluoric acid after 250 μg Be carrier and appropriate Al carrier were added (ensure Al in each sample is approximately 1000 μg). Al concentrations in duplicated aliquots of the parent solutions by subsampling were measured by Inductively Coupled Plasma-Optical Emission Spectrometry (ICP-OES). Be and Al were then subsequently separated from solution by successive anionic and cationic resin extraction and precipitation. Finally, BeO and Al_2O_3, obtained from these precipitates by drying and heating at 850 °C were mixed with niobium and silver respectively, and packed into a hollow copper target. The samples were analyzed for $^{10}Be/^{9}Be$ and $^{26}Al/^{27}Al$ ratios by accelerator mass spectrometry (AMS) at Scottish Universities Environmental Research Centre (SUERC). The laboratory blank of $^{10}Be/^{9}Be$ and $^{26}Al/^{27}Al$ ratios were 1.11×10^{-15} and 1.089×10^{-15} respectively. The analytical uncertainties (reported as 1σ) include those associated with AMS counting statistics and internal error (3%), chemical blank and ICP-OES internal error (5%).

4. RESULTS

Table 1 presents measured ^{10}Be and ^{26}Al concentrations and calculated erosion rates and effective exposure ages with analytical errors. All samples were normalized relative to 07KNSTD standard with ^{10}Be/^{9}Be and ^{26}Al/^{27}Al ratios of 2.79×10^{-11} and 4.11×10^{-11} (Nishiizumi, 2004; Nishiizumi et al., 2007) respectively. Erosion rates and effective exposure ages were determined from the ^{10}Be and ^{26}Al concentration using the Cronus online calculator (available at http://hess.ess.washington.edu/, Balco et al., 2008). We assumed a rock density of 2.7 g/cm^3, and the topographic shielding factor of 1. Erosion rates and effective exposure ages were calculated using the time dependent scaling scheme from Lal (1991) and Stone (2000). If the erosion rates have changed in the past, one would obtain mean erosion rates for the duration of the effective exposure ages (Lal et al., 2004), which defined as the duration time of removing ~0.6 m (equal to absorption depth) materials. Here the effective exposure ages vary from 53 ka to 140 ka, deduced from ^{10}Be concentrations (Table 1). The erosion rates from ^{10}Be concentrations range between 4.5 m/Ma and 12.4 m/Ma, with an average of 7.3 ± 2.6 m/Ma, similar to those from ^{26}Al concentrations. BJ-2 sampled at Yabulai Mountain front shows a highest erosion rate of 12.4 m/Ma.

A plot of ^{26}Al/^{10}Be versus ^{10}Be concentrations (Fig. 3) shows the exposure history of rocks (Lal, 1991). Samples fall into the steady state erosion island indicate the persistent exposure of rocks. Otherwise, either the rock has been buried or the data is unreliable. Also, if there are processes that remove thicknesses of material greater than absorption depth, the measured ^{26}Al/^{10}Be ratios would be smaller, the steady state assumption would be invalid (Cockburn et al., 1999). The effect of these mass wasting events can be avoided by sampling on the flat bedrock or the summit of residue hills without large scattering debris around. All samples located in the steady state erosion island within errors, but short-term burial episodes of < 100 ka timescales would also be possible, because massive sand are transported from the Badain Jaran Desert to the Tengger Desert and Ulan Buh Desert by west wind (Yang et al., 2014). However, erosion rates deduce from ^{10}Be and ^{26}Al concentrations are consistent (the differences between ^{26}Al-derived rates and ^{10}Be-derived rates

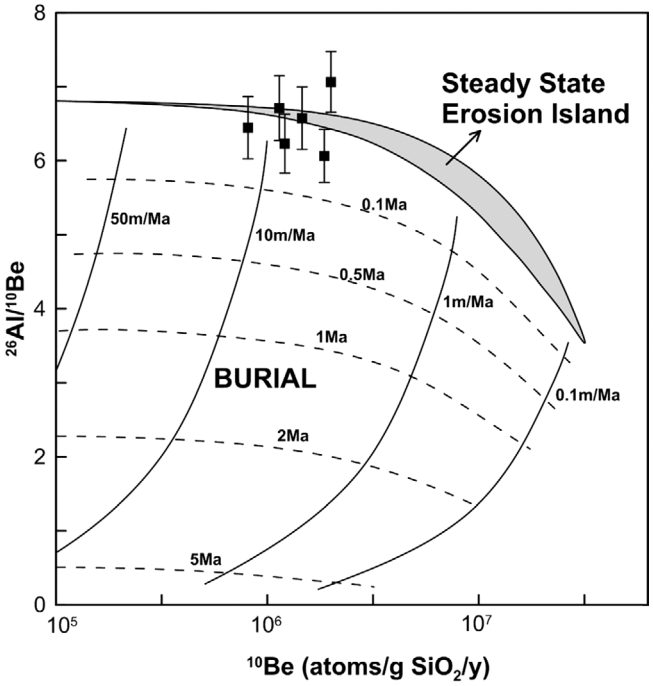

Fig. 3. Plot of ^{26}Al/^{10}Be versus ^{10}Be concentrations. The dashed line denote theoretical equal burial age line, and the straight line represent the path that rocks are buried after reaching an erosion state on the upper curve. All samples located within the steady state erosion island suggest the continuous exposure history of rocks.

are ~6%), which indicates such burial episodes caused by sand cover have insignificant effect on surface erosion rates, and the sampled surfaces have minimal complexity in their exposure history. Besides, cold and arid climate would extend the distribution of the sand dunes (Gao et al., 2006). The general trend of the climate of study area is becoming colder and direr, accompanied by alternation of cold dry and warm humid stages. Thus sand dunes have not extended farther than its present limit. Due to strong west wind, the mobile sand is hard to accumulate on flat granitic bodies and affect the bedrock erosion rate.

5. DISCUSSION

5.1. Tectonic and Climatic Control on Erosion

Both tectonics and climate affect surface erosion and change

Table 1. ^{10}Be and ^{26}Al concentrations and calculated erosion rates and effective exposure ages with analytical errors

Sample	Latitude (°N)	Longitude (°E)	Altitude (m)	^{10}Be conc. (10^6 atoms/g)	^{26}Al conc. (10^6 atoms/g)	^{26}Al/^{10}Be	^{10}Be erosion rate (m/Ma)	^{26}Al erosion rate (m/Ma)	Effective exposure age (ka)
BJ-1	39.1231	102.5605	1555	1.86 ± 0.05	11.28 ± 0.59	6.06 ± 0.36	5.0 ± 0.4	5.3 ± 0.6	125 ± 11
BJ-2	39.9240	103.6758	1569	0.81 ± 0.03	5.22 ± 0.28	6.44 ± 0.42	12.4 ± 1.1	12.8 ± 1.3	53 ± 4
BJ-3	39.8920	103.7564	1518	1.21 ± 0.04	7.54 ± 0.41	6.23 ± 0.40	7.9 ± 0.7	8.2 ± 0.9	84 ± 7
BJ-4	40.7667	103.1434	1475	2.00 ± 0.05	14.13 ± 0.74	7.07 ± 0.41	4.5 ± 0.4	3.9 ± 0.4	140 ± 12
BJ-5	40.7260	103.1975	1427	1.14 ± 0.04	7.65 ± 0.42	6.71 ± 0.44	7.9 ± 0.7	7.6 ± 0.8	83 ± 7
BJ-6	40.2574	104.4155	1466	1.46 ± 0.05	9.60 ± 0.52	6.58 ± 0.42	6.2 ± 0.6	6.0 ± 0.6	104 ± 9

https://doi.org/10.1007/s12303-018-0010-7

the landform. The erosion rate of the Badain Jaran Desert is 7.3 m/Ma which is higher than ^{10}Be erosion rate of granitic rocks in other tectonically stable and arid areas, for instance, the central Atacama Desert 0.2–0.4 m/Ma (MAP: ~10 mm/a, Placzek et al., 2010), Paran Plain 0.2–0.8 m/Ma (MAP: 50 mm/a, Matmon et al., 2009), Australian Eyre Peninsula 0.7 m/Ma (MAP: 325 mm/a, Bierman and Caffee, 2002), Antarctica 0.1–1 m/Ma (MAP: 50 mm/a, Nishiizumi et al., 1991), Namib Desert 3.5 ± 1.8 m/Ma (MAP: 10–100 mm/a, Bierman and Caffee, 2001). The calculated rate is similar to those of New Mexico Pajarito Plateau 1–11 m/Ma (MAP: 500 mm/a, Albrecht et al., 1993), the interior of Tibetan Plateau 9 ± 8 m/Ma (MAP: 100 mm/a, Lal et al., 2004), and central Turkey 5.8–9.3 m/Ma (MAP: 421 mm/a, Sarikaya et al., 2015). However, the Badain Jaran Desert erosion rate is lower than tectonic active regions in a varied MAP range, such as Australian Flinders mountain 14.2 m/Ma (254 mm/a, Quigley et al., 2007), Northwestern Tibetan Plateau 12.3 ± 6.7 m/Ma (50 mm/a, Kong et al., 2007), Israel Nahal Yael 29 m/Ma (30 mm/a, Clapp et al., 2000), Arizona Yuma Wash 30 m/Ma (90 mm/a, Clapp et al., 2002) and East Kunlun mountain 2000 m/Ma (350 mm/a, Lal et al., 2004). Even considering the 10–20% uncertainties (Lal, 1991; Nishiizumi et al., 2007; Chmeleff et al., 2010) from calculating parameters including nuclides production rate, rock density, decay constant and attenuation length, the arid regions in tectonically active settings are still with remarkably high erosion rate (Fig. 4).

Quigley et al. (2007) proposed that ^{10}Be could trace the recent landscape change responding to neotectonism, which may be a dominant control on bedrock erosion rate in intraplate settings, and pointed out two mechanisms for enhanced erosion rates: over-steepening of rivers and hillslopes caused by headward migration of fault-generated bedrock knickpoint and co-seismic shaking which could fragmentize the rock. For this study, no rivers or paleo-channels was observed near the sampling sites.

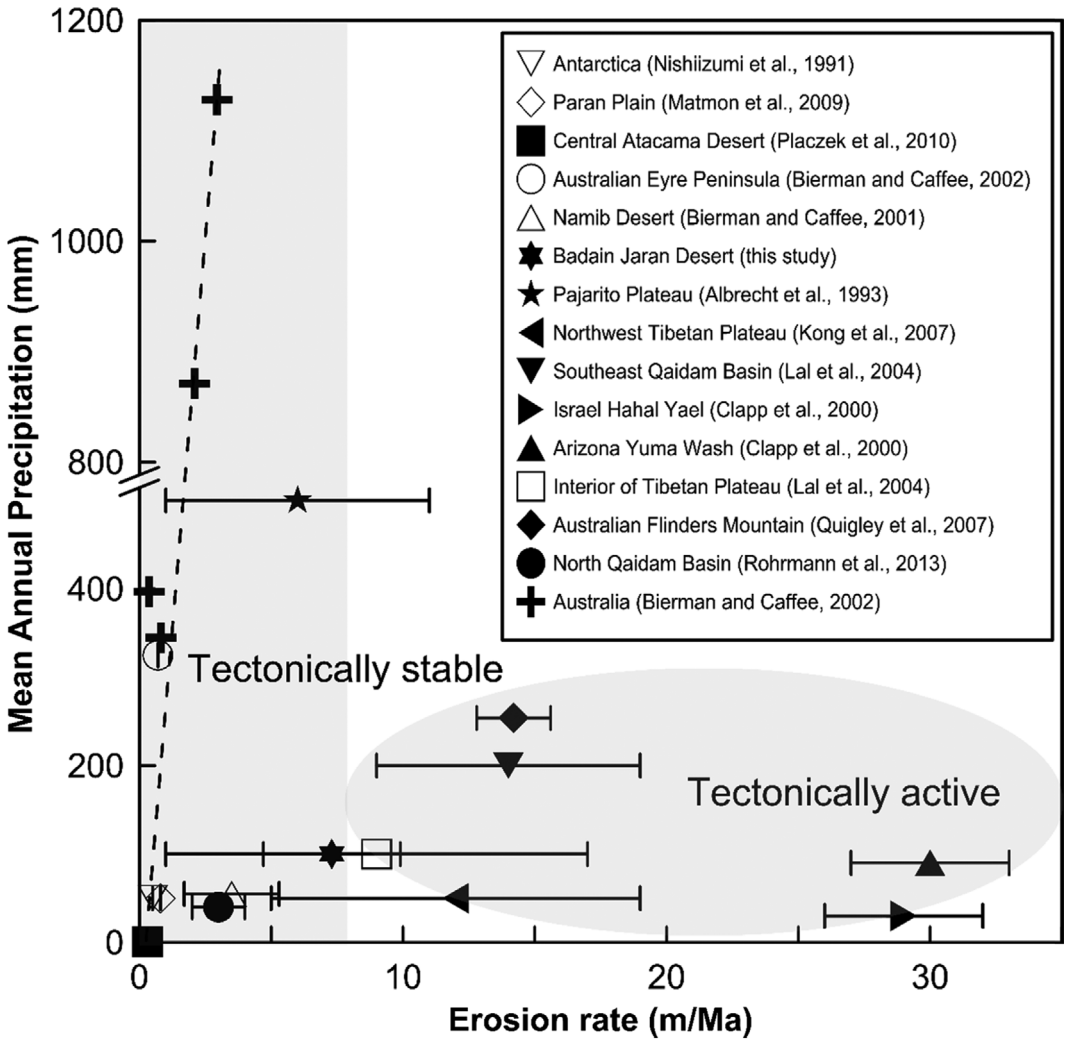

Fig. 4. Plot of erosion rate and Mean Annual Precipitation of this study and previous studies for bedrocks. Comparison of bedrock erosion rates deduced from cosmogenic nuclides concentrations in arid regions with contrasting tectonic activities can be made in this figure. A subtle positive relationship (dashed line) exists between erosion rates and precipitations in tectonically stable terrains.

In addition, the mean annual evaporation is ~1000 mm/y from water surface and ~100 mm/y from dune surface (Yang et al., 2010), which are much higher than the annual precipitation of 37–118 mm/y. Almost no surface water discharge on this areas. Thus the river over-steepening or incision effect is negligible. The highest erosion rate of 12.4 m/Ma (BJ-2), sampled at the Yalulai Mountain front, may have a connection with the active Yabulai Mountain Fault and the seismic events. BJ-3 was sampled ~50 km from Yabulai Mountain Fault, the influence of fault activities by the above mechanisms on surface erosion rate is limited. The erosion rates of both BJ-2 and BJ-3 are in the same order of magnitude with other rates at the stable desert plain. These indicate that the desert is relatively stable and the influence of seismic or fault activity of Yabulai Mountain fault on the regional-scale erosion rate is insignificant. Wind erosion could be the primary mechanism enhancing the erosion rate, as the study area is widely characterized by aeolian landforms (Yang et al., 2003). An additional and alternative explanation could be the wetter and warmer climate in the history here, which promoted chemical weathering thus erosion process.

Wind is an important erosion agent in arid, windy and barren regions (Thomas, 1998). A recent study from Rohrmann et al. (2013) reported a granite erosion rate of 3 m/Ma determined from ^{10}Be concentration in Qaidam Basin, which is adjacent to the study area. The Qaidam Basin with one-third of the basin floor exposes yardangs, has a significant wind eroded volume which equivalents to a volume of one-sixth of the Loess Plateau since Pleistocene (Rohrmann et al., 2013), the granite erosion there mainly results from wind force. However, the wind erosion rate of 3 m/Ma is still lower than 7.3 m/Ma and may not completely explain the relative high erosion rate in the Badain Jaran Desert.

The chemical weathering process, which mainly controlled by regional precipitation and temperature (Oliva et al., 2003; Anderson et al., 2007), transferred bedrock into soluble constitutes and weathering residuals through chemical alteration and dissolution of constituent minerals, in other words, weathering process is a bedrock porosity increasing process (Navarre et al., 2013), which makes rocks vulnerable to be physically eroded. Physical erosion and chemical weathering are correlated in many weathering-limited environmental settings (e.g., Riebe et al., 2004; Larsen et al., 2014). Schoonejans et al. (2016) demonstrate the coupling of chemical weathering and total denudation in semiarid climate conditions. Larsen et al. (2014) suggest that the emergence of bare bedrocks in tectonically active landscapes is controlled in large part by climate. At the sampling sites, weathering rates are slower than erosion rates, loose soils are stripped and bare rock surfaces appeared. The extremely dry climate retards the chemical weathering processes, sparse weathering products here are removed immediately by the strong prevailing west wind, and bedrocks are continuously exposed. The weathering-limited situation here suggests that the rock erosion rates are partially restricted by the slower weathering rates.

Based on a number of paleo-climatic and geologic studies, it is likely that the climatic evolution trend of the Badain Jaran Desert is in shifting of cold dry and warm wet climate, with a sub-trend of becoming colder and drier since late Pleistocene because of the fluctuation of East Asia monsoon, winter monsoon and westerly circulation (Herzschuh et al., 2004; Yang et al., 2004; Li et al., 2005; Gao et al., 2006; Yang et al., 2010; Ma et al., 2012; Liu et al., 2015). Pollen assemblages documented in the Chagelebulu Geological Profile in south desert indicated that the vegetation cover changed to grassland with open forest, and precipitation was generally high with a prevailing wet climate between 130 ka and 70 ka BP (Yang, 2000; Gao et al., 2006), and evidences from Ili loess from cemented calcareous layers in the Badain Jaran Desert also suggested a warm and humid climatic conditions during 40–30 ka BP, the annual mean precipitation at that time was between 60–300 mm greater than today (Yang et al., 2004). Thus, the assumption can be made that the periodically warmer and wetter climate, increased the water vapor including rainfall, fog, frost and groundwater seepage, accelerated the rock weathering process, and thus promote the erosion rate simultaneously in the Badain Jaran Desert (Viles and Goudie, 2013).

Bierman and Caffee (2002) documented that positive correlation exists between bedrock erosion rate and mean annual precipitation in Australia (Fig. 4). In a modern arid climate background, it is reasonable to infer that the erosion process in the Badain Jaran Desert is partly governed by relatively intense chemical weathering during warmer and wetter climate regime in history. Further investigation is necessary to explore the erosion mechanism in this area.

5.2. Implications for Landform Evolution

Generally, the regional landform evolution can be initially explored by surface erosion and incision history of local river system. Based on Optically Stimulated Luminescence (OSL) dating of paleochannel terraces, Liu (2014) proposed a long-term incision rate (12 m/Ma) for Suhongtu River in northern Badain Jaran Desert. Assuming this rate can be regarded as the mean incision rate for the whole drainage system over Pleistocene, we speculatively estimate that regional erosion surface increased their relative relief only about 12 m since Pleistocene. However, complications exist, first almost 80% of the area of the Badain Jaran Desert is covered by sand dunes where erosion rate is

 https://doi.org/10.1007/s12303-018-0010-7

difficult to be estimate. Second aeolian transportation contribute to sand deposit on surface, these would reduce the erosion rate of bedrocks. Finally wind erosion shows significantly diverse rates (3–400 m/Ma) on bedrocks with different tensile strength (Rohrmann et al., 2013). The estimated granitic bedrock erosion may not be a completely reliable indicator to explore the landform evolution of the Badain Jaran Desert. Nonetheless, our result is consistent with granite erosion rate of 7.2 m/Ma deduced from cosmogenic ^{21}Ne concentrations in Shapotou areas between Tengger Desert and Loess Plateau (Ma et al., 2016), which suggests the regional-scale granitic rock erosion rate of ~7 m/Ma could be representative of the Badain Jaran Desert and its surrounding areas.

In addition, sand transported from the Badain Jaran Desert to the Tengger Desert and Ulan Buh Desert by the dominant west wind through several corridors. The annual total amount of sand transported from the Badain Jaran Desert to Tengger Desert is over 5×10^6 t (Yang et al., 2014). Except mega-dunes and flat sandy land which account for 92% of the desert areas (Zhu et al., 2010), at most 8% of the desert floor expose bedrocks. We assume a regional-scale erosion rate of bedrocks of 7.3 m/Ma and rock density of 2.7 g/cm^3, and estimate an eroded mass flux of 7.8×10^4 t/y. The materials produced by bedrocks in the Badain Jaran Desert only account for 1.6% of the sand transported to Tengger Desert. Also considering the dunes in the Badain Jaran Desert have continued their growth since 130 ka to 4 ka, according to the OSL ages, and grown mostly during wet periods (Yang et al., 2010; Liu et al., 2015), the desert dunes are likely sand sink rather than sand source. Thus, the estimates are indicative of the other sand sources of the Badain Jaran Desert to balance the materials that formed the dunes and transported to Tengger and Ulan Buh Desert. This estimates support the previous view that the aeolian deposits in the Badain Jaran Desert are predominantly derived from Qilian Mountains, Altai Mountains and Mongolian Gobi (Hu and Yang, 2016).

6. CONCLUSION

Erosion rates of granitic bedrocks in extremely arid Badain Jaran Desert have been determined by in situ produced cosmogenic ^{10}Be and ^{26}Al. A plot of the steady state erosion island indicates the persistent exposure of bedrocks. The estimated erosion rate of 7.3 m/Ma is significantly higher than most of the reported data with similar settings. Wind erosion and the periodically warmer and wetter climate in the regional history are considered as the dominant mechanisms accounting for this relatively high erosion rate in the Badain Jaran Desert. The influences of the sand dunes, aeolian deposits and diverse erosion rates of different bedrocks complicate the exploration of landform evolution with bedrock erosion rate. Nonetheless, estimation could be made that the materials contribution of bedrock erosion products is negligible in the Badian Jaran Desert, which indicates massive exogenous materials input to the desert.

ACKNOWLEDGMENTS

This work was financially supported by the "Strategic Priority Research Program" of the Chinese Academy of Sciences (Grant No. XDB15010405), Natural Science Foundation of China (Grant No. 41402323, 91747202, 41772380 and 41730857) and the National Basic Research Program of China ("973 Program", Grant No. 2013CB956401). Wenjing Liu acknowledges support from the international postdoctoral exchange fellowship program (Grant No. 20140045). The paper benefited much from insightful comments from the handling editor and anonymous reviewers.

REFERENCES

Albrecht, A., Herzog, G., Klein, J., Dezfoulyarjomandy, B., and Goff, F., 1993, Quaternary erosion and cosmic-ray exposure history derived from ^{10}Be and ^{26}Al produced in situ – an example from Pajarito Plateau, Valles caldera region. Geology, 21, 551–554.

An, C., Feng, Z., and Barton, L., 2006, Dry or humid? Mid-Holocene humidity changes in arid and semi-arid China. Quaternary Science Reviews, 25, 351–361.

Anderson, S., Blanckenburg, F., and White, A., 2007, Physical and chemical controls on the critical zone. Elements, 3, 315–319.

Balco, G., Stone, J., Lifton, N., and Dunai, T., 2008, A complete and easily accessible means of calculating surface exposure ages or erosion rates from ^{10}Be and ^{26}Al measurements. Quaternary Geochronology, 3, 174–195.

Belton, D.X., Brown, R.W., Kohn, B.P., Fink, D., and Farley, K.A., 2004, Quantitative resolution of the debate over antiquity of the central Australian landscape: implications for the tectonic and geomorphic stability of cratonic interiors. Earth and Planetary Science Letters, 219, 21–34.

Bierman, P. and Caffee, M., 2001, Slow rates of rock surface erosion and sediment production across the Namib Desert and Escarpment, Southern Africa. American Journal of Science, 301, 326–358.

Bierman, P. and Caffee, M., 2002, Cosmogenic exposure and erosion history of Australian bedrock landforms. Geological Society of America Bulletin, 114, 787–803.

Chen, B. and Xu, W., 2006, Sinistral strike-slip faults along the southern Alashan margin and eastwards extending of the Altun fault. Seismology and Geology, 28, 319–324. (in Chinese with English abstract)

Chmeleff, J., Blanckenburg, F., Kossert, K., and Jakob, D., 2010, Determination of the ^{10}Be half-life by multi-collector ICP-MS and liquid scintillation counting. Nuclear Instruments and Methods in Physical Research, 263, 192–199.

Clapp, E., Bierman, P., Schick, A., Lekach, J., Enzel, Y., and Caffee, M.,

2000, Sediment yield exceeds sediment production in arid region drainage basins. Geology, 28, 995–998.

Clapp, E., Bierman, P.R., and Caffee, M., 2002, Using ^{10}Be and ^{26}Al to determine sediment generation rates and identify sediment source areas in an arid region drainage basin. Geomorphology, 45, 89–104.

Cockburn, H., Brown, R.W., Summerfield, M., and Seidl, M., 2000, Quantifying passive margin denudation and landscape development using a combined fission-track thermochronology and cosmogenic isotope analysis approach. Earth and Planetary Science Letters, 179, 429–435.

Cockburn, H., Seidl, M.A., and Summerfield, M., 1999, Quantifying denudation rates on inselbergs in the central Namib Desert using in situ-produced cosmogenic ^{10}Be and ^{26}Al. Geology, 27, 399–402.

Darby, B.J., Ritts, B.D., Yue, Y., and Meng, Q., 2005, Did the Altyn Tagh fault extend beyond the Tibetan Plateau? Earth and Planetary Science Letters, 240, 325–435.

Dong, C., Wang, N., Chen, J., Li, Z., Chen, H., and Chen, L., 2016, New observational and experimental evidence for the recharge mechanism of the lake group in the Alxa Desert, north central China. Journal of Arid Environments, 124, 48–61.

Fujioka, T. and Chappell, J., 2011, Desert landscape processes on a timescale of millions of years, probed by cosmogenic nuclides. Aeolian Research, 3, 157–164.

Fujioka, T., Chappell, J., Yatsevich, M.H., Fifield, K., and Fabel, D., 2005, Global cooling initiate stony deserts in central Australia 2–4 Ma, dated by cosmogenic ^{21}Ne-^{10}Be. Geology, 33, 993–996.

Gao, L., He, J.G., Zhang, S., Kong, H., Tian, M., and Huang, F., 2013, Study on crustal stability of Alashan area. World Nuclear Geoscience, 30, 237–244. (in Chinese with English abstract)

Gao, Q., Tao, Z., Li, B., Jin, H., Zou, X., and Zhang, Y., 2006, Palaeomonsoon variability in the southern fringe of the Badain Jaran Desert, China, since 130 ka BP. Earth Surface Processes and Landforms, 31, 265–283.

Herzschuh, U., Tarasov, P., Wunnemann, B., and Kai, H., 2004, Holocene vegetation and climate of the Alashan Plateau, NW China, reconstructed from pollen data. Palaeogeography Palaeoclimatology Palaeoecology, 211, 1–17.

Hu, F. and Yang, X., 2016, Geochemical and geomorphological evidence for the provenance of aeolian deposits in the Badain Jaran Desert, northwestern China. Quaternary Science Reviews, 131, 179–192.

Kohl, C. and Nishiizumi, K., 1992, Chemical isolation of quartz for measurement of in-situ-produced cosmogenic nuclides. Geochimica et Cosmochimica Acta, 56, 3583–3587.

Kong, P., Na, C., Fink, D., Ding, L., and Huang, F., 2007, Erosion in Northwest Tibet from in situ produced cosmogenic ^{10}Be and ^{26}Al in bedrock. Earth Surface Processes and Landforms, 32, 116–125.

Korschinek, G., Bergmaier, A., Faestermann, T., Gerstmann, U.C., Knie, K., Rugel, G., Wallner, A., Dillmann, I., Dollinger, G., Ch. Lierse von Gostomski, Kossert, K., Maiti, M., Poutivtsev, M., and Remmert, A., 2010, A new value for the half-life of ^{10}Be by heavy-ion elastic recoil detection and liquid scintillation counting. Nuclear Instruments and Methods in Physics Research, 268, 187–191.

Lal, D., 1991, Cosmic ray labeling of erosion surfaces: in situ nuclide production rates and erosion models. Earth and Planetary Science Letters, 104, 424–439.

Lal, D., Harris, N., Sharma, K., Gu, Z., Ding, L., and Liu, T., 2004, Erosion history of the Tibetan Plateau since the last interglacial: constraints from the first studies of cosmogenic ^{10}Be from Tibetan bedrock. Earth and Planetary Science Letters, 217, 33–42.

Larsen, I.J., Almond, P.C., Eger, A., Stone, J., Montgomery, D., and Malcolm, B., 2014, Rapid soil production and weathering in the Southern Alps, New Zealand. Science, 343, 637–640.

Li, S., Gao, Z., Yan, C., Li, Z., Dong, R., and Wen, H., 2005, A recent study on sedimentary sequence of southeastern Badain Jaran Desert since 150 ka BP. Journal of Desert Research, 25, 457–464. (in Chinese with English abstract)

Liu, M.E., 2014, Study on the Quaternary river landscape in Yabrai Mountain, Alax Area, Inner Mongolia. Master Thesis, University of Geosciences, Beijing, 49 p. (in Chinese with English abstract)

Liu, W., Lai, P., Wang, X., Fan, L., Wang, L., and Tian, Z., 2015, Growing pattern of mega-dunes in the Badain Jaran Desert in China revealed by luminescence ages. Quaternary International, 410, 111–118.

Ma, J., Wang, Y., Zhao, Y., Jin, X., Ning, N., and Edmunds, W., 2012, Spatial distribution of chloride and nitrate within an unsaturated dune sand of a cold-arid desert: implications for paleoenvironmental records. Catena, 96, 68–75.

Ma, Y., Wu, Y., Li, D., Zheng, D., Zheng, W., and Zhang, H., 2016, Erosion rate in the Shapotou area, northwestern China, constrained by in situ-produced cosmogenic ^{21}Ne in long-exposed erosional surfaces. Quaternary Geochronology, 31, 3–11.

Martin, H.A., 2006, Cenozoic climatic change and the development of the arid vegetation in Australia. Journal of Arid Environments, 66, 533–563.

Matmon, A., Simhai, O., Amit, R., Haviv, I., Porat, N., and Mcdonald, E., 2009, Desert pavement-coated surfaces in extreme deserts present the longest-lived landforms on Earth. Geological Society of America Bulletin, 121, 688–697.

Navarre, A., Cole, D., Rother, G., Jin, L., Buss, H., and Brantley, S., 2013, Porosity and surface area evolution during weathering of two igneous rocks. Geochimica et Cosmochimica Acta, 109, 400–413.

Nishiizumi, K., 2004, Preparation of ^{26}Al AMS standards. Nuclear Instruments and Methods in Physics Research, s223–224, 388–392.

Nishiizumi, K., Imamura, M., Caffee, M., Southon, J., Finkel, R., and Mcaninch, J., 2007, Absolute calibration of ^{10}Be AMS standards. Nuclear Instruments and Methods in Physics Research, 258, 403–413.

Nishiizumi, K., Kohl, C.P., Arnold, J., Klein, J., Find, D., and Middleton, R., 1991, Cosmic ray produced ^{10}Be and ^{26}Al in Antarctic rocks: exposure and erosion history. Earth and Planetary Science Letters, 104, 440–454.

Norris, T.L., Gancarz, A.J., Rokop, D.J., and Thomas, K.W., 1983, Half-life of Al-26. Journal of Geophysical Research Atmospheres, 14, 331.

Oliva, P., Viers, J., and Dupré, B., 2003, Chemical weathering in granitic environments. Chemical Geology, 202, 225–256.

Placzek, C.J., Matmon, A., Granger, D., Quade, J., and Niedermann, S.,

 https://doi.org/10.1007/s12303-018-0010-7

2010, Evidence for active landscape evolution in the hyper-arid Atacama from multiple terrestrial cosmogenic nuclides. Earth and Planetary Science Letters, 295, 12–20.

Quigley, M., Sandiford, M., Fifield, L., and Alimanovic, A., 2007, Landscape responses to intraplate tectonism: Quantitative constraints from ^{10}Be nuclide abundances. Earth and Planetary Science Letters, 261, 120–133.

Riebe, C.S., Kirchner, J.W., and Finkel, R.C., 2004, Erosional and climatic effects on long-term chemical weathering rates in granitic landscapes spanning diverse climate regimes. Earth and Planetary Science Letters, 224, 547–562.

Rohrmann, A., Heermance, R., Kapp, P., and Cai, F., 2013, Wind as the primary driver of erosion in the Qaidam Basin, China. Earth and Planetary Science Letters, 374, 1–10.

Sarikaya, M.A., Çiner, A., and Zreda, M., 2015, Fairy chimney erosion rates on cappadocia ignimbrites, Turkey: insights from cosmogenic nuclides. Geomorphology, 234, 182–191.

Schoonejans, J., Vanacker, V., Opfergelt, S., Ameijeiras-Marino, Y., and Christl, M., 2016, Kinetically limited weathering at low denudation rates in semiarid climatic conditions. Journal of Geophysical Research Earth Surface, 121, 336–350.

Small, E., Anderson, R.S., Repka, J., and Finkel, R., 1997, Erosion rates of alpine bedrock summit surfaces deduced from in situ ^{10}Be and ^{26}Al. Earth and Planetary Science Letters, 150, 413–425.

Stone, J.O., 2000, Air pressure and cosmogenic isotope production. Journal of Geophysical Research, 105, 753–759.

Thomas, D., 1998, Arid zone geomorphology: process, form and change in dry lands. Sedimentary Geology, 116, 275.

Viles, H.A. and Goudie, A.S., 2013, Weathering in the central Namib Desert, Namibia: controls, processes and implications. Journal of Arid Environments, 93, 20–29.

von Blanckenburg, F., 2005, The control mechanisms of erosion and weathering at basin scale from cosmogenic nuclides in river sediment. Earth and Planetary Science Letters, 237, 462–479.

Wateren, F.M. and Dunai, T.J., 2001, Lake Neogene passive margin denudation History –cosmogenic isotope measurements from the Central Namib Desert. Global and Planetary Change, 30, 271–307.

Yang, B., Shi, Y., Braeuning, A., and Wang, J., 2004, Evidence for a warm-humid climate in arid northwestern China during 40–30 ka BP. Quaternary Science Reviews, 23, 2537–2548.

Yang, X.P., Liu, T., and Xiao, H., 2003, Evolution of mega-dunes and lakes in the Badain Jaran Desert, Inner Mongolia, China during the last 31,000 years. Quaternary International, 104, 99–112.

Yang, X.P., Ma, N., Dong, F., Zhu, Q., Xu, B., and Ma, B., 2010, Recharge to the inter-dune lakes and Holocene climatic changes in the Badain Jaran Desert, western China. Quaternary Research, 73, 10–19.

Yang, Y., Qu, Q., Shi, J., Liu, Y., Zhang, M., and Tang, Y., 2014, Wind regime and sand transport in the corridor between the Badain Jaran and Tengger Deserts, central Alxa Plateau, China. Aeolian Research, 12, 143–156.

Yu, J.X., Zhen, W.J., Lei, Y., Shao, X., Ge, W., Ma, Y., and Li, J., 2013, Neotectonics and kinetics along the Yabulai range front fault in the south Alashan block and its implications for regional tectonics. Seismology and Geology, 35, 731–743. (in Chinese with English abstract)

Zhang, Z., Dong, Z., and Li, C., 2015, Wind regime and sand transport in China's Badain Jaran Desert. Aeolian Research, 17, 1–13.

Zhu, J.F., Wang, N.A., Chen, B., Dong, Y., and Zhang, A., 2010, Study on the boundary and the area of the Badain Jaran Desert based on remote sensing imagery. Progress in Geography, 29, 1087–1094. (in Chinese with English abstract)